# Pharmacological inhibition of MAGL attenuates experimental colon carcinogenesis

# Pharmacological inhibition of MAGL lipase attenuates experimental colon carcinogenesis

Ester Pagano[1*], Francesca Borrelli[1*#], Pierangelo Orlando[2,3*], Barbara Romano[1*], Martina Monti[4], Lucia Morbidelli[4], Gabriella Aviello[5], Roberta Imperatore[6*], Raffaele Capasso[1*], Fabiana Piscitelli[6*], Lorena Buono[6,7], Vincenzo Di Marzo[6*#], Angelo A. Izzo[1*]

[1]Department of Pharmacy, University of Naples Federico II, Naples, Italy; [2]Institute of Protein Biochemistry, Naples, Italy; [3]Institute of Applied Sciences & Intelligent Systems, National Research Counsil, Pozzuoli (NA), Italy; [4]Department of Life Sciences, University of Siena, Siena, Italy; [5]National Children's Research Centre, Our Lady's Children's Hospital Crumlin, Dublin 12, Dublin, Ireland; [6]Institute of Biomolecular Chemistry, National Research Council , Pozzuoli (NA), Italy; [7]Centro de Biología Molecular "Severo Ochoa", Consejo Superior de Investigaciones Científicas-UAM, 28049, Cantoblanco, Spain. [*]Endocannabinoid Research Group

[#]**Corresponding Authors:** Francesca Borrelli: Department of Pharmacy, University of Naples Federico II, via D Montesano 49, 80131 Naples, Italy; email: franborr@unina.it, tel +39-081.6784665, Fax.: +39-081678403; Vincenzo di Marzo: Institute of Biomolecular Chemistry, National Research Council , Pozzuoli (NA), Italy; email: vdimarzo@icb.cnr.it, tel +39-0818675193 Fax.: +39-0818041770

**Graphical abstract**

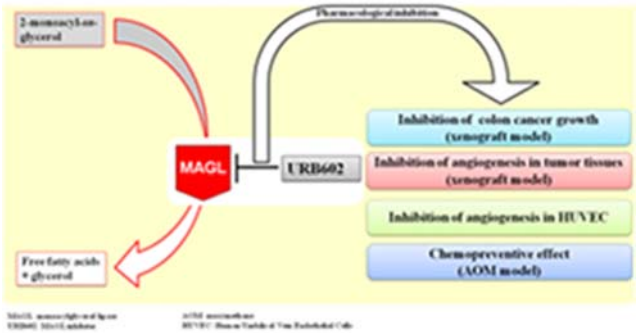


**ABSTRACT**

Colorectal cancer (CRC) is a major health problem in Western countries. The endocannabinoid 2-arachidonoyl-glycerol (2-AG) exerts antiproliferative actions in a number of tumoral cell lines, including CRC cells. Monoacylglycerol lipase (MAGL), a serine hydrolase that inactivates 2-AG, is highly expressed in aggressive human cancer cells. Here, we investigated the role of MAGL in experimental colon carcinogenesis. The role of MAGL was assessed *in vivo* by using the xenograft and the azoxymethane models of colon carcinogenesis; MAGL expression was evaluated by RT-PCR and immunohistochemistry; 2-AG levels were measured by liquid chromatography mass spectrometry; angiogenesis was evaluated in tumor tissues [by microvessel counting and by investigating the expression of vascular endothelial growth factor (VEGF) and fibroblast growth factor-2 (FGF-2) proteins] as well as in human umbilical vein endothelial cells (HUVEC); cyclin D1 was evaluated by RT-PCR. MAGL and 2-AG were strongly expressed in tumor tissues. The MAGL inhibitor URB602 reduced xenograft tumor volume, this effect being associated to down-regulation of VEGF and FGF-2, reduction in the number of vessels and down-regulation of cyclin D1. In HUVEC, URB602 exerted a direct antiangiogenic effect by inhibiting FGF-2 induced proliferation and migration, and by modulating pro/anti-angiogenic agents. In experiments aiming at investigating the role of MAGL in chemoprevention, URB602 attenuated azoxymethane-induced

preneoplastic lesions, polyps and tumors. MAGL, possibly through modulation of angiogenesis, plays a pivotal role in experimental colon carcinogenesis. Pharmacological inhibition of MAGL could represent an innovative therapeutic approach to reduce colorectal tumor progression.

**ABBREVIATIONS:**

2-arachydonoyl glycerol, 2-AG; aberrant crypt foci, ACF; anandamide, AEA; azoxymethane, AOM; bovine serum albumin, BSA; colon adenocarcinoma cell line, HCT116; colorectal cancer, CRC; dimethyl sulphoxide, DMSO; Dulbecco's modified Eagle's medium, DMEM; endothelial growth medium-2, EGM-2; fatty acid amide hydrolase, FAAH; fetal calf serum, FCS; fibroblast growth factor-2, FGF-2; foetal bovine serum, FBS; human umbilical vein endothelial cell line, HUVEC; intraperitoneally, i.p.; monoacylglycerol lipase, MAGL; oleoylethanolamide, OEA; palmitoylethanolamide, PEA; phosphate buffer solution, PBS; tris-buffered saline, TBS; vascular endothelial growth factor, VEGF.

**Keywords**

Cannabinoid receptor, colorectal cancer, cancer prevention, lipid metabolism.

## 1. INTRODUCTION

Colorectal cancer (CRC) is the most prevalent gastrointestinal malignancy worldwide [1,2]. It has been estimated that, in 2015, it will be the third most common cause of cancer-related deaths in USA with a prediction of 132,700 new diagnosed cases [3]. It has been known that sporadic CRC develops, in the majority of cases, as a consequence of the sequential accumulation of genetic alterations and epigenetic modulations [4,5]. The disease begins with the generation of pre-neoplastic lesions, known as aberrant crypt foci (ACF), and, through the formation of polyps, develops into an advanced adenoma with high-grade dysplasia and then progresses to an invasive cancer [6]. The microenvironment plays a crucial role in the tumor growth and a considerable number of key transduction signals are involved in tumor microenvironment progression, such as angiogenesis and cycle progression. In particular, it is largely reported the importance of angiogenesis for the development of solid tumors because the dissemination of tumors requires new blood vessel growth [7,8]. Despite clear progress in physiopathology and cure of colon cancer, current therapeutic interventions may fail to prevent disease progression to metastatic dissemination. Therefore, it is crucial to identify different molecular actors playing a key role in CRC oncogenesis.

Monoacylglycerol lipase (MAGL) is a serine hydrolase that converts monoacylglicerols to glycerol and fatty acid. The enzyme is localized in different areas of brain and in peripheral tissues, including the gastrointestinal tract [9-11]. MAGL is up-regulated in aggressive human ovarian, prostate, breast cancer cells and in primary tumors, where it promotes migration, invasion, survival, and *in vivo* tumor growth [12,13].

MAGL plays a predominant role in catalyzing the hydrolysis of the endocannabinoid 2-arachydonoyl glycerol (2-AG) [14-16], whereas other enzymes are more involved in the hydrolysis of the endocannabinoid anandamide and related acylethanolamides (i.e. palmitoylethanolamide and oleoylethanolamide [17,18]. 2-AG is generated "*on demand*" through *stimulus*-dependent cleavage of membrane phospholipid precursors and its levels are regulated by the balance between its

production and degradation [19]. This endocannabinoid is involved in a variety of physiological and physiopathological processes. Relevant to this study, 2-AG has been shown to exert antiproliferative effects in a number of cancer cell lines [20-22], including colorectal cancer cells [23]; conversely, reducing endogenous 2-AG-levels increases cell invasion [24]. Importantly, the increase of endogenous 2-AG levels as a consequence of MAGL inhibition was shown to reduce prostate cancer invasion *in vitro* [25].

Our understanding of how MAGL can impact on cancer progression is so far hindered by under-reported and controversial [26,27], having been suggested to mediate both cancerogenic [28] and anti-cancerogenic effects [29]. Furthermore, the effect and role of MAGL in relation to 2-AG production and angiogenesis have been not evaluated to date. Therefore, in the present study we have investigated the role of MAGL in colon carcinogenesis by evaluating the potential chemopreventive and curative effect of the selective MAGL inhibitor URB602. Specifically, the effects of URB602 on tumor progression, 2-AG levels and angiogenesis were evaluated.

## 2. MATERIALS AND METHODS

### 2.1. Drugs and reagents

Azoxymethane (AOM) was purchased from Sigma (Milan, Italy). URB602 and Matrigel™ were obtained from Cayman Chemical (Cabru SAS, Arcore, Italy) and BD Biosciences (Buccinasco, Milan, Italy), respectively. All reagents for cell cultures were obtained from Sigma, Bio-Rad Laboratories (Milan, Italy) and Microtech Srl (Naples, Italy). The vehicles used for *in vivo* (10% ethanol, 10% Tween-20, 80% saline, 2 ml/kg) and *in vitro* (0.1% DMSO) experiments had no effect on the responses under study.

### 2.2. Cell culture

The human colon adenocarcinoma cell line (HCT116, ATCC from LGC Standards, Milan, Italy) and the human umbilical vein endothelial cell line (HUVEC, Promocell, Heidelberg, Germany) were used. Cells were routinely maintained in 75 $cm^2$ polystyrene flasks, at 37 °C in a 5% $CO_2$ atmosphere, in Dulbecco's modified Eagle's medium (DMEM) for HCT116 or in endothelial

growth medium (EGM-2) for HUVEC. DMEM was supplemented with 10% foetal bovine serum (FBS), 100 U/ml penicillin, 100 μg/ml streptomycin, 1% non-essential amino acids and 2 mM L-glutamine. EGM-2, containing VEGF, $R^3$-IGF-1, hEGF, hFGF, hydrocortisone, ascorbic acid, heparin and GA-1000 (Clonetics, Cambrex Bio Science Walkersville, USA) was supplemented with 10% FBS. Cells were used at passage 20-27 for HCT 116 and 1-10 for HUVEC. The medium was changed every 48 h in conformity with the manufacturer's protocols.

**2.3. Animals**

Male ICR mice (weighting 25–30 g) and athymic nude female 4-weeks old mice were purchased from Harlan Italy (S. Pietro al Natisone, UD, Italy). All mice were used after 1 week-acclimation period (temperature 23±2 °C; humidity 60%, free access to water and food). Athymic female mice, fed *ad libitum* with sterile mouse food, were maintained under pathogen-free conditions. The experimental protocol was evaluated and approved by the Institutional Animal Ethics Committee for the use of experimental animals and conformed to guidelines for the safe use and care of experimental animals in accordance with the Italian D.L. no.116 of 27 January 1992 and associated guidelines in the European Communities Council (86/609/ECC and 2010/63/UE).

**2.4. Colorectal cancer xenograft model**

HCT 116 cells ($2.5x10^6$) were injected subcutaneously into the right flank of each athymic mouse for a total volume of 200 μl [50% cell suspension in phosphate buffer solution (PBS) and 50% Matrigel™]. Ten days after inoculation (once tumors had reached a size of 250-300 $mm^3$), mice were randomly assigned to control and treated groups, and treatments were initiated. Tumor size was measured every day by digital caliper, and tumor volume was calculated according to the modified formula for ellipsoid volume (volume = $\pi/6 \times$ length $\times$ $width^2$). Mice were euthanized when the endpoint tumor volume was of 2000 $mm^3$. The MAGL inhibitor URB602 [30], at the dose of 5 mg/kg, was given intraperitoneally (i.p.) every day for all the duration of the experiment. URB602 dose was selected on the basis of previous published work which showed selective inhibitory effects of URB602 on MAGL enzyme without psychoactive effects [31]. Xenograft

tumor tissue as well as healthy tissue were collected and analyzed after 8 days of treatment. Healthy tissue derived from contralateral flank (i.e. the flank not injected with xenografted cells) which includes skin, muscle, connective tissue and nerves.

**2.5. Quantitative (real-time) RT-PCR analysis**

Healthy tissues and tumors collected from xenografted mice were immediately immersed into RNA Later and stored at -20°C until analysis. HCT 116 and tissues were homogenized in 1.0 mL of TRIzol (Invitrogen) following the manufacturer's instructions and a quantitative mRNA expression was performed (for more details and primer sequences, see Supplementary material).

**2.6. Immunohistochemistry**

The animals were deeply anesthetized with pentobarbital (100 mg/kg) and then perfused transcardially with 0.9% saline solution for 5 min, followed by 100 ml of fixative containing 4% paraformaldehyde (wt/vol)/0.1 M phosphate buffer (pH 7.4). After fixation tumor slices were cut with a Leica CM3050S cryostat in serial frozen sections (10 μm-thick) and processed for immunofluorescence. Immunohistochemical study of MAGL expression in tumor slices collected from xenografted mice was performed by incubation of sections with goat anti-MAGL (1:200, Abcam, Milan, Italy) revealed by specific Alexa-594 secondary donkey anti-IgGs antibody (Invitrogen Life Technology, Paisley, UK) and counterstained with 40 ,6-diamidino-2-phenylindole. Immunoreactivity for MAGL was analyzed by DMI6000 microscope equipped with appropriate filters and deconvolution software MetaMorph LAS AF 2.2.0 software (Leica, Germany).

**2.7. Identification and quantification of endocannabinoids and related acylethanolamides**

Endocannabinoids [anandamide (AEA) and 2-arachidonoylglycerol (2-AG)], palmitoylethanolamide (PEA) and oleoylethanolamide (OEA) levels were measured in tumor and healthy tissues of xenografted mice as well as in HCT116 cells (used for inoculation) by isotope dilution liquid chromatography-atmospheric pressure-chemical ionization mass spectrometry, as previously described [32].

**2.8. Immunostaining for CD31**

Collected tumors were immediately embedded in Tissue-Tek O.C.T. (Sakura, San Marcos, CA), cooled in isopentane and frozen in liquid nitrogen for immunostaining and histological analysis. Seven μm-thick cryostat sections from a xenograft tumors were stained with hematoxylin and eosin and sections were used for immunohistochemical staining with anti CD31 (Chemicon, Millipore, Milan, Italy) antibody. For immunohistochemistry, cryostat sections were firstly fixed in acetone at -20° C and incubated for 10 min in 3% $H_2O_2$, washed (3 x 5 min) in Tris-buffered saline (TBS) and then incubated in a Blocking reagent (KIT Immunoperoxidase Secondary Detection System, Chemicon, Millipore, Milan, Italy). Mouse monoclonal anti-CD31 antibody diluted 1:100 in TBS, 0.05% bovine serum albumin (BSA) was applied. Negative controls were produced by eliminating the primary antibodies from the diluents. Sections were then washed (3 x 5 min in TBS) and incubated for 10 min in the appropriate species–specific biotinylated secondary antibodies (goat anti mouse IgG, KIT Immunoperoxidase Secondary Detection System, Chemicon). Following washings (3 x 5 min in TBS), the sections were incubated for 10 min in streptavidin-conjugated HRP and then exposed to 3,3-diaminobenzidine tetrahydrocloride (DAB, detection kit, Millipore, Milan, Italy) for 8 min to produce a brown reaction product. Finally, sections were counterstained in hematoxylin and mounted in Aquatex (Merck, Milan, Italy) [33].

For CD31 immunofluorescence labelling, sections were fixed in acetone, and aspecific binding sites were blocked by using 3% BSA. Slides were incubated with a rat anti-mouse CD31 antibody (Millipore, Billerica, USA). Immunoreactions were revealed by using FITC anti-rat secondary antibodies. Images were analyzed using Nikon Eclypse T200, and quantification of human CD31 and vessel lumina were performed counting 10 random field/section for slides.

**2.9. Western blot analysis**

The expression of vascular endothelial growth factor (VEGF), fibroblast growth factor-2 (FGF-2) and endostatin was assessed by western blot analyses in xenograft tumor tissue of animals treated or not with URB602. Samples were fragmented in liquid nitrogen, lysed in Cell Lytic buffer

(Invitrogen) and centrifuged at 14000 rpm for 15 min. Supernatant was collected and protein concentration was determined by Bio-Rad Protein Assay (Bio-Rad); lysate aliquots containing 50 μg of proteins were separated by SDS-PAGE (4-12% PA, NuPAGE, Invitrogen) and transferred to a nitrocellulose membrane using iBlot2 (Life Technologies, Monza, Italia). After blocking in 5% w/v nonfat dry milk (1X PBS) buffer, membranes were incubated overnight with anti-FGF-2 (1:1000, Upstate), polyclonal anti-VEGF (1:1000, Millipore) or anti-endostatin (1:1000, Millipore); after washing, secondary antibody anti-mouse or anti-rabbit IgG (1:2500, Promega), linked to horseradish peroxidase, was added. The signal was visualized by enhanced chemiluminescence using Chemidoc XRS (Biorad) and analyzed using Quantity One Software version 4.6.3. The membranes were probed with anti-β-actin antibody (1:1000, Sigma) to normalize the results, which were expressed as ratio of densitometric analysis of each protein/β-actin bands.

**2.10. Proliferation assay in HUVEC**

For proliferation assay, HUVEC were seeded in 96 multiwell plates at a density of 1 x $10^3$ cells per well and after adherence (3-4 h) they were serum starved for 12 hours. Cells under basal condition [0.1% fetal calf serum (FCS)] or stimulated for 24 h with either 1% FCS or FGF-2 (20 ng/ml) were treated with URB602 (0.1 and 1 μM). Cells were then fixed, stained and randomly counted at 20 x magnification [34]. Data are expressed as counted cells/well.

**2.11. Migration assay in HUVEC**

HUVEC were seeded into 24-well plates (1 x $10^5$ cells/well) and incubated for 24 h to confluence. Then, the monolayer was scraped using a sterile micropipette tip to create a wound of ± 1 mm width. Cells were washed twice with PBS, and fresh medium containing test substances was added with ARA-C (2.5 μg/ml) to inhibit cell proliferation. Images of the wound in each well were acquired from 0 to 8 h under a phase contrast microscope at 20 x magnification. After 8 h cells were stained with Hoechst 33342 and image acquisition and analysis were performed by a Nikon digital camera DS-5MC and NIS Element software, using a Nikon Eclipse TE 300 inverted microscope (Nikon, Tokyo, Japan). Results are expressed as percentage of area of wound [35].

### 2.12 Quantification of angiogenesis modulators in HUVEC

FGF-2 and endostatin levels were measured in conditioned media by ELISA kits (R&D System, Minneapolis, MN, USA). HUVEC were exposed to URB602 (1 μM, 18 h) in 0.1% or 1% FCS. Cell culture supernatants were collected, stored at -80C°C and analysed following manufacturer instructions. Data are reported as pg/ml (FGF-2) or ng/ml (endostatin) (means± SEM). Experiments were run in triplicate.

### 2.13. Colorectal cancer azoxymethane (AOM) model

Mice were randomly divided into the following three groups (10 animals/group): group 1 (control) was treated with vehicles; group 2 was treated with azoxymethane (AOM) plus the vehicle used to dissolve URB602 and group 3 was treated with AOM plus URB602 (5 mg/kg).

AOM (40 mg/kg in total, i.p.) was administered in mice at the single dose of 10 mg/kg at the beginning of the first, second, third and fourth week. URB602 at the dose of 5 mg/kg was given i.p. three times a week starting one week before the first administration of AOM. All animals were euthanized by asphyxiation with $CO_2$ three months after the first injection of AOM. Based on our laboratory experience, this time (at the used dose of AOM) was associated with the occurrence of a significant number of aberrant crypt foci (ACF, which are considered pre-neoplastic lesions), polyps and tumors [36]. Pre-neoplastic and neoplastic lesions were evaluated on isolated colons as previously reported [36]. Briefly, ACF were identified for their greater size, larger and elongated luminal opening, thicker lining, compression of the surrounding epithelium and more darkly staining with methylene blue. The criterion to distinguish polyps from tumors was established considering the main characteristic features of these two lesions (i.e. crypt distortion around a central focus and increased distance from luminal to basal surface of cells for polyps and high grade of dysplasia with complete loss of crypt morphology for tumors) [37].

### 2.14. Statistical analysis

Statistical analysis has been carried out using GraphPad Prism 5.0 (GraphPad Software, San Diego, CA, USA). Data are expressed as the mean±standard error mean (SEM) of *n* experiments. To

determine statistical significance, Student's t test was used for comparing a single treatment mean with a control mean, and analysis of variance followed by a Tukey-Kramer multiple comparisons test was used for analysis of multiple treatment means. The *Post hoc* test was performed only if F achieved the $P<0.05$ level of significance [38]. *P* values<0.05 were considered significant.

## 3. RESULTS

### 3.1.MAGL expression in human colorectal carcinoma (HCT 116) cells and xenograft tumor tissue

In order to elucidate the role of MAGL in colorectal tumorigenesis, we generated xenografts by inoculating human colorectal cancer (HCT 116) cells in athymic mice.

Although human MAGL mRNA was weakly expressed in the HCT 116 cells, the transcriptional analysis of the xenograft tumor tissue showed high gene expression of human MAGL (Figure 1A). As expected, human MAGL mRNA was undetectable in the mouse contralateral paw, used as negative control (data not shown). Moreover, immunostaining revealed high expression of MAGL protein in tumor tissue (figure 1B), although the precise localization of the enzyme within the cell was not detectable.

### 3.2. The MAGL inhibitor URB602 reduced xenograft tumor growth

We evaluated the potential antitumor curative effect of the MAGL inhibitor URB602 by using a xenografted tumor model generated as described above. On day 10 after s.c. cell inoculation, all the mice developed tumors, with a mean volume (± SEM) of 288±37 $mm^3$. Thereafter, mice were treated daily either with vehicle or URB602 (5 mg/kg, i.p.). As shown in figure 2, the administration of URB602 significantly reduced tumor growth compared to vehicle. Eight days after drug administration, the average tumor volume in the control group was 1980±269 $mm^3$, whereas the average tumor volume in the URB602-treated group was 956±180, exhibiting a 52% of tumor growth inhibition (figure 2).

### 3.3. Effect of URB602 on 2-AG levels in healthy and tumor tissues from xenografted mice

The levels of 2-AG found in tumor tissue of xenografted mice were higher than those detected in HCT116 cell lines (figure 3A, insert) and in healthy tissues derived from the contralateral flank of xenografted mice (i.e. the flank not injected with xenografted cells) (figure 3A). URB602, at the daily i.p. dose of 5 mg/kg, significantly increased, by approximately four-folds, the levels of 2-AG in healthy tissues, but it was not able to further increase the already elevated 2-AG levels in tumor tissues (figure 3A).

In order to verify URB602 selectivity, we measured the levels of anandamide and related acylethanolamides following URB602 treatment. The MAGL inhibitor did not significantly change anandamide levels in both healthy and tumor tissues (figure 3B). Similarly, levels of PEA and OEA, both in healthy (PEA pmol/mg: control: 105.6±46.64, URB602: 220.2±120.1; OEA pmol/mg: control: 11.02±3.86, URB602: 23.12±6.447; n=5 mice for each experimental group) and in tumor (PEA pmol/mg: control: 121.1±41.79, URB602: 124.5±44.19; OEA pmol/mg: control: 12.0±1.597, URB602: 9.50±2.132; n=5 mice for each experimental group) tissues, were unchanged. Collectively these results suggest the selectivity of URB602 for MAGL *vs* acylethanolamide-hydrolyzing amidases.

### 3.4. URB602 drives in vivo angiogenesis output in xenograft tumor tissue

Figure 4 shows the panel of angiogenesis modulators following URB602 treatment. URB602 decreased the expression of pro-angiogenic factors (i.e. VEGF and FGF-2), while it had no effect on the expression of endostatin, an anti-angiogenic modulator in tumor tissues. We also evaluated, by RT-PCR, mRNA expression of VEGF, the most important pro-angiogenic factor [39,40]. Results, depicted in the insert to figure 4, showed that URB602 treatment decreased VEGF mRNA transcription.

Tumor samples were also analyzed for microvessel density (by counting CD-31 positive neovessels), structure and composition. All these parameters were significantly reduced by URB602 (figure 5), thus suggesting antiangiogenetic effects *in vivo*.

### 3.5. Direct antiangiogenic effect of URB602 in HUVEC

To verify if URB602 exerts a direct antiangiogenic effect, the MAGL inhibitor was tested in HUVEC stimulated with FGF-2 or 1% FCS. Both FGF-2 or 1% FCS stimulation (24 h) increased cell proliferation (figure 6). The stimulated cell proliferation was inhibited by non-cytotoxic concentrations of URB602 (0.1 and 1 μM) (figure 6A). In un-stimulated cells (0.1% FCS), URB602, at the 0.1 μM concentration, stimulated proliferation (figure 6A). Concentrations higher than 1 μM were not used because they resulted in a cytotoxic effect.

The antiangiogenic effect of URB602 was corroborated by the observation that the inhibitor, at the 1 μM concentration, significantly reduced migration of adherent cells induced by both FGF-2 and 1% FCS (8 h incubation). Specifically, the angiogenic factors reduced wound area and URB602 impaired the closure of wounds [see the quantification of scratch reported as percentage of healing in figure 6B (top) and the representative pictures in figure 6B (bottom)]. In un-stimulated cells (0.1% FCS), URB602 increased migration (figure 6B).

Finally, we analyzed the balance of pro- and anti-angiogenic factors released by HUVEC in the culture media. The increase of FBS concentration (from 0.1 % to 1%) induced a significant increase in FGF-2 release and a significant decrease in endostatin levels, as a sign of endothelial activation (Figure 7, see white columns). Both these changes were restored by URB602 treatment (Figure 7). Collectively, such data suggest a direct effect of URB602 on endothelial cells, through the modulation of endothelial cells functional response and production of autocrine/paracrine modulators of angiogenesis.

### 3.6. Cyclin D1 of xenograft tumor tissue was down-regulated in URB602-treated mice

In order to investigate the antiproliferative effects of URB602 *in vivo*, the expression of two cell cycle regulator genes (i.e. cyclin-D1 and p27KIP) was evaluated in tumor xenograft tissues.

URB602 decreased the mRNA expression of cyclin-D1 (normilized fold expression±SEM: vehicle: 2.574±0.28; URB602: 1.0±0.02*; n=4, *p<0.05 vs vehicle), a factor that, by promoting cell DNA synthesis and cell growth, stimulates cancer cell proliferation [41]. No significant effect of URB602 on the cycle-negative regulator p27KIP was observed (data not shown).

**3.7. URB602 exerts chemopreventive effects in the AOM model of colon carcinogenesis**

The carcinogenic agent AOM, given alone, up-regulated colonic mRNA MAGL expression (mRNA fold expression of MAGL±SEM: control: 1.0±0.06, AOM: 1.7±0.04*; n=4 *p<0.05 vs control) and induced the expected appearance of ACF (figure 8A), polyps (figure 8B) and tumors (figure 8C) after a three month treatment. URB602 (5 mg/kg), given i.p. without the AOM-initiating treatment, was unable to induce ACF, polyps and tumors, thus demonstrating that this compound is devoid of tumor-initiating activity in this experimental model (data not shown). However, URB602 significantly reduced AOM-induced ACF (figure 8A) and tumors (figure 8C), while it showed a trend to decrease the number of polyps (figure 8B).

**4. DISCUSSION**

Colorectal cancer is an important health problem across the world. Despite significant advancements in prevention, diagnosis and cure, morbidity and mortality rates remain sadly high, calling for the identification of new strategies, including the recognition of innovative targets for pharmacological intervention. MAGL and its main substrate 2-AG have been involved in a number of tumor types [13,20-22,25]. However, the role of MAGL in colorectal cancer physiopathology is both under-researched and controversial [28,29], with no study attempting to relate MAGL with its main substrate 2-AG and angiogenesis. Here we have shown that MAGL and 2-AG are present in tumor tissue and that pharmacological inhibition of MAGL results in chemopreventive (AOM model) and curative (xenograft model) effects in colon carcinogenesis.

### 4.1. Presence of MAGL and 2-AG in the xenograft tumor tissue

Monoacylglycerols such as the endocannabinoid 2-AG, are metabolized to free fatty acids and glycerol by MAGL. MAGL has been shown to be up-regulated in aggressive compared to non-aggressive tumor cell lines as well as in primary tumors [12,42]. Here, we have shown that tumour tissues generated by injection of human colorectal cancer (HCT116) cells in nude mice express both mRNA MAGL and its related protein. Due to the use of specific human antibodies, it is very likely that the detected MAGL mRNA in the tumor xenograft derives from human epithelial cells, possibly underwent to phenotypic changes during tumor implantation and growth. Others have shown that MAGL was up-regulated in colorectal cancer patient tissues [29].

Because MAGL is the main enzyme responsible of 2-AG degradation, we measured its levels in the tumor mass. 2-AG, which is known to exert antiproliferative effects in colorectal cancer cells [23], was shown to be elevated in the mouse colon of AOM-induced ACF [32] as well as in colorectal polyps and tumors in patients [23]. In our study we have revealed, in tumor tissues, amounts (300 pmol/mg of lipid extract) of 2-AG that were about four-fold higher than those detected in HCT116 cells and healthy tissues derived from the contralateral flank of xenografted mice (i.e. the flank not injected with xenografted cells).

### 4.2. Effect of URB602 on 2-AG levels, tumor progression and angiogenesis (xenograft model)

In order to evaluate tumor progression, angiogenesis and tumor 2-AG levels associated to MAGL inhibition, we selected the MAGL inhibitor URB602, i.e. the first compound reported with selectivity for MAGL over fatty acid amide hydrolase (FAAH) [17]. Although the *in vitro* selectivity of high concentrations of this compound (2-AG *vs* anandamide hydrolysis) has been questioned [43], its functional selectivity has been demonstrated by the ability to elevate 2-AG levels in hippocampal slice cultures without affecting levels of other endocannabinoid-related molecules [16,44]. In contrast to directly-activating $CB_1$ receptor agonists, URB602, given i.p. at doses less than 10 mg/kg, did not induce catalepsy and hypothermia [31].

*i) Effect of URB602 on 2-AG levels in xenograft tumor tissues.*

We have found that URB602, at the daily dose of 5 mg/kg, which is significantly lower than that found to be active at, e.g., reducing upper intestinal transit [10], showed only a non-significant trend toward an increase in 2-AG levels in the xenograft tumor tissue. The failure of URB602 to significantly increase 2-AG levels could be due to the high levels of the endocannabinoid already present in the tumor tissue (see above). In fact, under the same experimental conditions, URB602 increased 2-AG levels in healthy tissues, where the basal levels of 2-AG are not so high like in tumor mass. Importantly, in this set of experiments, we found that URB602 significantly and selectively increased (by approximately four-fold) 2-AG levels, without significantly affecting the levels of anandamide (non-significant two-fold increase) and the related acylethanolamides (i.e.palmitoylethanolamide and oleoylethanolamide).

*ii) Effect of URB602 on xenograft tumor progression*

Previous studies have shown that 2-AG as well as inhibitors of 2-AG hydrolysis exerted anti-tumorigenic (antiproliferative, inhibition of invasion and cell migration) effects in a number of cancer cell lines, including prostate, ovarian, breast and melanoma cells [12,41]. However, the role of MAGL in colorectal cancer cells is controversial. Ye and colleagues found that colorectal cancer cell growth and invasion were inhibited by pharmacological and siRNA mediated MAGL knock-down [29]. By contrast, a more recent paper highlighted the potential tumor suppressive role of MAGL in colorectal cancer cell lines, based on the findings that over-expression of MAGL suppressed colony formation in cell lines and knockdown of MAGL resulted in increased Akt phosphorylation [28]. In the present study we have shown that URB602, at the daily dose of 5 mg/kg, reduced the growth of tumors generated by xenograft injection of colorectal cancer cells in athymic mice. It is important to further emphasize that URB602 reduced tumor growth at a dose devoid of central side effects [31] and which selectively inhibits the metabolism of 2-AG without affecting the hydrolysis of anandamide and related acylethanolamide (present results, see above). Consistent with our data, Ye and colleagues showed that JZL184, a potent and selective MAGL

inhibitor, reduced tumor formation generated by xenograft injection of colorectal cancer (Caco-2) cells in nude mice [29].

*iii) Effect of URB602 on angiogenesis and proliferation in xenograft tumor tissues*

A fundamental feature of tumor progression is the accomplishment of abundant vascular development to sustain the growing tumor mass [8]. Therefore, we evaluated the impact of URB602 on a number of angiogenesis markers in tumor-bearing mice. Although no specific study on 2-AG or MAGL on angiogenesis exists, cannabinoids, in addition to their cancer cell death promoting effects, have been also shown to normalize tumor vasculature [45-48]. In cancer cells, cannabinoids inhibit the activation of the vascular endothelial growth factor (VEGF) cascade, which is considered the most important and well-characterized pathway contributing to angiogenesis [38,39], and a number of elements of this cascade are down-regulated by cannabinoids, for example, in skin carcinomas, gliomas and thyroid carcinomas [see 49, for review].

Here, we have provided a number of evidence suggesting that URB602 acts via inhibition of angiogenesis. Indeed: URB602 i) reduced the expression of VEGF, which is considered the most important and the well-characterized contributor to angiogenesis [38,39]; ii) reduced density, structure and composition of tumor vessels. Furthermore, using HUVEC we were able to recapitulate *in vitro* the anti-angiogenic effect of URB602. To the best of our knowledge, this represents the first demonstration about the involvement of MAGL and of its main substrate 2-AG in angiogenesis.

Lastly, our results show that the beneficial effect of URB602 was associated to down-regulation of cyclin D1, a specific cyclin required for tumor progression. Down-regulation of cyclin D1 is known to restrict the cell cycle progression to the G0/G1 phase. Conversely, cyclin D1 over-expression has been observed in 68.3% of human colorectal cancer, suggesting a role in human colorectal tumorigenesis [50]. Others have shown that the putative endocannabinoid noladin ether down-regulated cyclin D1 expression in cancer prostate cells and that Met-F-anandamide (a synthetic analogue of anandamide) in combination with the FAAH inhibitor URB597, induces G0/G1 cell

cycle arrest by down-regulating cyclin D1 [51]. However, in the present study no significant effect of URB602 on the cycle-negative regulator p27KIP was observed.

### 4.3. Effect of URB602 in the axoxymethane (AOM) model of colon carcinogenesis

In a different set of experiments, we evaluated the effect of URB602 in a model of colon carcinogenesis induced by AOM. This model is extensively used to study the mechanisms underlying human sporadic colon cancer as well as to evaluate drug potential chemopreventive effects [52]. AOM administration in mice causes the formation of preneoplastic lesions (ACF), polyps and tumors. We have previously shown that the pharmacological enhancement of endocannabinoid levels (through inhibition of anandamide hydrolysis by the FAAH inhibitor N-arachidonoylserotonin) as well as the cannabinoid receptor agonist HU-210 attenuated the development of ACF in the mouse colon [42]. Here, we have shown that MAGL is over-expressed in the colon of AOM-treated mice and, more importantly, that URB602 reduced, approximately by one half, the number of ACF, polyps and tumors.

## 5. CONCLUSIONS

In the present study we have shown that MAGL and its main substrate 2-AG are present in the colorectal cancer tumor tissues and that a pharmacological inhibition of the enzyme by URB602, which selectively increases 2-AG *in vivo*, resulted in chemopreventive and curative effects in murine models of colon carcinogenesis. The curative effect of URB602 was associated to inhibition of angiogenesis and to down-regulation of cyclin D1, a marker of cell proliferation. Furthermore, URB602 exerted a direct antiangiogenic effect in human endothelial cells. The present results contribute to elucidate the physiopathological role of MAGL in colon carcinogenesis and thus may offer novel future pharmacological opportunities for colon cancer prevention and cure.

## Author contribution

Ester Pagano was responsible for acquisition, analysis and interpretation of data, conception and design and redaction of the manuscript. Ester Pagano, Barbara Romano, Raffaele Capasso and Gabriella Aviello performed in vivo experiments; Piero Orlando and Lorena Buono performed RT-

PCR analysis and Roberta Imperatore generated the immunohistochemistry data. Fabiana Piscitelli evaluated endocannabinoid levels and Lucia Morbidelli and Martina Monti generated the angiogenesis data. Angelo A. Izzo, Vincenzo Di Marzo and Francesca Borrelli were responsible for conception and design, analysis and interpretation of data, and critical reading of the manuscript.

**Acknowledgements**

This work was partly supported by Istituto Toscano Tumori (ITT) and ADLER PLASTIC SPA.

**REFERENCES**

[1] E.R. Fearon, Molecular genetics of colorectal cancer, Annu Rev Pathol. 6 (2011) 479-507.

[2] M. Malvezzi, P. Bertuccio, F. Levi, C. La Vecchia, E. Negri, European cancer mortality predictions for the year 2014, Ann Oncol. 25 (2014) 1650-1656.

[3] R.L. Siegel, K.D. Miller, A. Jemal, Cancer statistics, 2015, CA Cancer J Clin. 65 (2015) 5-29.

[4] M. Pancione, A. Remo, V. Colantuoni, Genetic and epigenetic events generate multiple pathways in colorectal cancer progression. Patholog Res Int. 2012 (2012) 509348.

[5] V.V. Lao, W.M. Grady, Epigenetics and colorectal cancer, Nat Rev Gastroenterol Hepatol. 8 (2011) 686-700.

[6] S.D. Markowitz, M.M. Bertagnolli, Molecular origins of cancer: Molecular basis of colorectal cancer, N Engl J Med. 361 (2009) 2449-2460.

[7] W. Risau, Mechanisms of angiogenesis, Nature. 386 (1997) 671-4.

[8] D. Hanahan, J. Folkman, Patterns and emerging mechanisms of the angiogenic switch during tumorigenesis, Cell. 86 (1996) 353-64.

[9] K. Ahn M.K. McKinney, B.F. Cravatt, Enzymatic pathways that regulate endocannabinoid signaling in the nervous system, Chem Rev. 108 (2008) 1687-707. Review.

[10] M. Duncan, A.D. Thomas, N.L. Cluny, A. Patel, K.D. Patel, B. Lutz, et al., Distribution and function of monoacylglycerol lipase in the gastrointestinal tract, Am J Physiol Gastrointest Liver Physiol. 295 (2008) G1255-65.

[11] A.A. Izzo, M. Camilleri, Cannabinoids in intestinal inflammation and cancer, Pharmacol Res. 60 (2009) 117-25.

[12] M.M. Mulvihill, D.K. Nomura, Therapeutic potential of monoacylglycerol lipase inhibitors, Life Sci. 92 (2013) 492-7.

[13] D.K. Nomura, J.Z. Long, S. Niessen, H.S. Hoover, S.W. Ng, B.F. Cravatt, Monoacylglycerol lipase regulates a fatty acid network that promotes cancer pathogenesis, Cell. 140 (2010) 49-61.

[14] T.P. Dinh, T.F. Freund, D. Piomelli, A role for monoglyceride lipase in 2-arachidonoylglycerol inactivation, Chem Phys Lipids, 121 (2002) 149-58. Review

[15] T.P. Dinh, S. Kathuria, D. Piomelli, RNA interference suggests a primary role for monoacylglycerol lipase in the degradation of the endocannabinoid 2-arachidonoylglycerol, Mol Pharmacol. 66 (2004) 1260-4.

[16] A.G. Hohmann, R.L. Suplita, N.M. Bolton, M.H. Neely, D. Fegley, R. Mangieri, et al., An endocannabinoid mechanism for stress-induced analgesia, Nature. 435 (2005) 1108-12.

[17] C.J. Fowler, Monoacylglycerol lipase - a target for drug development? Br J Pharmacol. 166 (2012) 1568-85.

[18] N. Ueda, K. Tsuboi, T. Uyama, Metabolism of endocannabinoids and related N-acylethanolamines: canonical and alternative pathways, FEBS J. 280 (2013) 1874-94.

[19] N. Murataeva, A. Straiker, K. Mackie, Parsing the players: 2-arachidonoylglycerol synthesis and degradation in the CNS, Br J Pharmacol. 171 (2014) 1379-91. Review.

[20] D. Melck, L. De Petrocellis, P. Orlando, T. Bisogno, C. Laezza, M. Bifulco, et al., Suppression of nerve growth factor Trk receptors and prolactin receptors by endocannabinoids leads to inhibition of human breast and prostate cancer cell proliferation. Endocrinology. 141 (2000) 118-26.

[21] M.A. Costa, B.M. Fonseca, E. Keating, N.A. Teixeira, G. Correia-da-Silva, 2-arachidonoylglycerol effects in cytotrophoblasts: metabolic enzymes expression and apoptosis in BeWo cells, Reproduction. 147 (2014) 301-11.

[22] O. Orellana-Serradell, C.E. Poblete, C. Sanchez, E.A. Castellón, I. Gallegos, C. Huidobro, et al., Proapoptotic effect of endocannabinoids in prostate cancer cells, Oncol Rep. 33 (2015) 1599-608.

[23] A. Ligresti, T. Bisogno, I. Matias, L. De Petrocellis, M.G. Cascio, V. Cosenza, et al., Possible endocannabinoid control of colorectal cancer growth, Gastroenterology. 125 (2003) 677-687.

[24] K. Nithipatikom, M.A. Isbell, M.P. Endsley, J.E. Woodliff, W.B. Campbell, Anti-proliferative effect of a putative endocannabinoid, 2-arachidonylglyceryl ether in prostate carcinoma cells, Prostaglandins Other Lipid Mediat. 94 (2011) 34-43.

[25] D.K. Nomura, D.P. Lombardi, J.W. Chang, S. Niessen, A.M. Ward, J.Z. Long, et al., Monoacylglycerol lipase exerts dual control over endocannabinoid and fatty acid pathways to support prostate cancer, Chem Biol. 18 (2011) 846-56.

[26] R. Schicho, M. Storr, Alternative targets within the endocannabinoid system for future treatment of gastrointestinal diseases, Can J Gastroenterol. 25 (2011) 377-83.

[27] A.A. Izzo, G.G. Muccioli, M.R. Ruggieri, R. Schicho, Endocannabinoids and the Digestive Tract and Bladder in Health and Disease, Handb Exp Pharmacol. 231 (2015) 423-47.

[28] H. Sun, L. Jiang, X. Luo, W. Jin, Q. He, J. An, et al., Potential tumor-suppressive role of monoglyceride lipase in human colorectal cancer, Oncogene. 32 (2013) 234-41.

[29] L. Ye, B. Zhang, E.G. Seviour, K.X. Tao, X.L. Liu, Y. Ling, et al., Monoacylglycerol lipase (MAGL) knockdown inhibits tumor cells growth in colorectal cancer. Cancer Lett. 307 (2011) 6-17.

[30] S.P. Alexander, H.E. Benson, E. Faccenda, A.J. Pawson, J.L. Sharman, M. Spedding, et al., The Concise Guide to PHARMACOLOGY 2013/14: enzymes, Br J Pharmacol. 170 (2013) 1797-867.

[31] F. Comelli, G. Giagnoni, I. Bettoni, M. Colleoni, B. Costa, The inhibition of monoacylglycerol lipase by URB602 showed an anti-inflammatory and anti-nociceptive effect in a murine model of acute inflammation, Br J Pharmacol. 152 (2007) 787-94.

[32] A.A. Izzo, G. Aviello, S. Petrosino, P. Orlando, G. Marsicano, B. Lutz, et al., Increased endocannabinoid levels reduce the development of precancerous lesions in the mouse colon, J Mol Med. 86 (2008) 89-98.

[33] F. Finetti, E. Terzuoli, E. Bocci, I. Coletta, L. Polenzani, G. Mangano, et al., Pharmacological inhibition of microsomal prostaglandin E synthase-1 suppresses epidermal growth factor receptor-mediated tumor growth and angiogenesis, PLoS One. 7 (2012) e40576.

[34] S. Donnini, R. Solito, A. Giachetti, H.J. Granger, M. Ziche, L. Morbidelli, Fibroblast growth factor-2 mediates Angiotensin-converting enzyme inhibitor-induced angiogenesis in coronary endothelium, J Pharmacol Exp Ther. 319 (2006) 515-22.

[35] M. Monti, S. Donnini, A. Giachetti, D. Mochly-Rosen, M. Ziche, deltaPKC inhibition or varepsilon PKC activation repairs endothelial vascular dysfunction by regulating eNOS post-translational modification, J Mol Cell Cardiol. 48 (2010), 746-56.

[36] F. Borrelli, E. Pagano, B. Romano, S. Panzera, F. Maiello, D. Coppola, et al., Colon carcinogenesis is inhibited by the TRPM8 antagonist cannabigerol, a Cannabis-derived non-psychotropic cannabinoid, Carcinogenesis. 35 (2014) 2787-97.

[37] G.P. Boivin, K. Washington, K. Yang, J.M. Ward, T.P. Pretlow, R. Russell, et al., Pathology of mouse models of intestinal cancer: consensus report and recommendations. Gastroenterology. 124 (2003) 762–77

[38] M.J. Curtis. R.A. Bond, D. Spina, A. Ahluwalia, S.P. Alexander, M.A. Giembycz, et al., Experimental design and analysis and their reporting: new guidance for publication in BJP, Br J Pharmacol. 172 (2015) 3461-71.

[39] M. Shibuya, Vascular Endothelial Growth Factor (VEGF) and Its Receptor (VEGFR) Signaling in Angiogenesis: A Crucial Target for Anti- and Pro-Angiogenic Therapies, Genes Cancer. 2 (2011) 1097-105.

[40] N. Ferrara, Vascular endothelial growth factor as a target for anticancer therapy, Oncologist. 9 (2004) Suppl 1, 2-10. Review.

[41] T. Motokura, A. Arnold, Cyclins and oncogenesis, Biochim Biophys Acta. 1155 (1993) 63–78.

[42] R. Van Dross, E. Soliman, S. Jha, T. Johnson, S. Mukhopadhyay, Receptor-dependent and receptor-independent endocannabinoid signaling: a therapeutic target for regulation of cancer growth. Life Sci. 92 (2013) 463-6.

[43] S. Vandevoorde, K.O. Jonsson, G, Labar, E. Persson, D.M. Lambert, C.J. Fowler, Lack of selectivity of URB602 for 2-oleoylglycerol compared to anandamide hydrolysis in vitro, Br J Pharmacol. 150 (2007) 186-91.

[44] A.R. King, A. Duranti, A. Tontini, S. Rivara, A. Rosengarth, J.R. Clapper, et al., URB602 inhibits monoacylglycerol lipase and selectively blocks 2-arachidonoylglycerol degradation in intact brain slices, Chem Biol. 14 (2007) 1357-65.

[45] C. Blázquez, M.L. Casanova, A. Planas, T. Gómez Del Pulgar, C. Villanueva, M.J. Fernández-Aceñero, et al., Inhibition of tumor angiogenesis by cannabinoids, FASEB J. 17 (2003) 529-31.

[46] S. Pisanti, P. Picardi, L. Prota, M.C. Proto, C. Laezza, P.G. McGuire, et al., Genetic and pharmacologic inactivation of cannabinoid CB1 receptor inhibits angiogenesis, Blood, 117 (2011) 5541-50.

[47] S. Pisanti, P. Picardi, A. D'Alessandro, C, Laezza, M. Bifulco, The endocannabinoid signaling system in cancer, Trends Pharmacol Sci. 34 (2013) 273-82.

[48] G. Velasco, S. Hernández-Tiedra, D. Dávila, M. Lorente, The use of cannabinoids as anticancer agents, Prog Neuropsychopharmacol Biol Psychiatry pii: S0278-5846 (2015) 00119-0.

[49] G. Velasco, C. Sánchez, M. Guzmán. Anticancer mechanisms of cannabinoids. Curr Oncol. 23 (2016) S23-32. Review.

[50] A.A. Bahnassy, A.R. Zekri, S. El-Houssini, A.M. El-Shehaby, M.R. Mahmoud, S. Abdallah, et al., Cyclin A and cyclin D1 as significant prognostic markers in colorectal cancer patients, BMC Gastroenterol. 4 (2004) 22.

[51] J. Ravi, A. Sneh, K. Shilo, M.W. Nasser, R.K. Ganju, FAAH inhibition enhances anandamide mediated anti-tumorigenic effects in non-small cell lung cancer by downregulating the EGF/EGFR pathway, Oncotarget. 5 (2014) 2475-86.

[52] C. Neufert, C. Becker, M.F. Neurath, An inducible mouse model of colon carcinogenesis for the analysis of sporadic and inflammation-driven tumor progression, Nat Protoc. 2 (2007) 1998-2004.

**FIGURE LEGENDS**

**Figure 1.** Expression of MAGL in HCT116 xenograft model. (A) *Homo s.* MAGL mRNA was evaluated by quantitative (real-time) RT-PCR analysis in human colorectal carcinoma (HCT 116) cells and in xenograft tumor tissues (mean ±SEM of 5 independent experiments) as described in the "Methods" section. Data was not statistically analyzed because cells are phenotypically different. The lower expression (HCT116 cells) 30.01 Cq vs background 37 Cq was put= 1 (B) Immunohistochemical analysis of MAGL in tumor tissue derived from xenograft model. Scale bars are indicated.

**Figure 2.** Inhibitory effect of URB602 on tumor formation induced by subcutaneous injection of HCT 116 cells into the right flank of athymic female mice. Tumor size was measured every day by a digital caliper, and tumor volume was calculated. URB602 (5 mg/kg, i.p.) treatment started 10 days after cell inoculation and it was administered every day until the sacrifice of the animals. Results represent the mean ± SEM. of 9-11 mice.*$p<0.05$ and ***$P<0.001$ *vs* vehicle-treated nude mice.

**Figure 3** Effect of URB602 on 2-arachydonylglycerol (2-AG, figure 3A) and anandamide (AEA, (figure 3B) levels in healthy tissues [derived from contralateral flank of the xenografted mice (i.e. the flank not injected with xenografted cells)] and in the tumor tissue (HCT116 xenograft model). The inserts show a comparison between the levels of 2-AG (insert to figure 3A) and anandamide (insert to figure 3B) in HCT116 cell lines and in xenograft tumor tissue. Data of the insert were not statistically analyzed because cells are phenotypically different. URB602 (5 mg/kg, i.p.) treatment started 10 days after cell inoculation and it was administered every day until the sacrifice of the animals. Assays were performed 8 days after the first injection of URB602 (i.e. the day of animal sacrifice). Results are mean ± SEM of 5 independent experiments for each experimental group. *$P<0.05$ *vs* vehicle-treated nude mice. Note that the possible explanation on why URB602 does not increase 2-AG levels is provided in the Discussion section. In addition, note that "healthy tissue"

does not represent a control for "tumor tissue" and, accordingly, no statistical analysis has been performed between these two experimental groups.

**Figure 4.** Effect of URB602 on endostatin, VEGF and FGF-2 expression in the tumor mass (HCT116 xenograft model). URB602 (5 mg/kg, i.p.) treatment started 10 days after cell inoculation and it was administered every day until the sacrifice of the animals. Assays were performed 8 days after the first injection of URB602. (A) Representative blots, B-D) results expressed as *ratio* of densitometric analysis of each protein/β-actin bands (means ± SEM of 3 tumors from three different mice. Each experiment was in triplicate). ***P<0.001 *vs* vehicle-treated nude mice. The insert shows the mRNA expression of VEGF in the tumor tissue (HCT116 xenograft model) from animals treated or not by URB 602. *P<0.05 vs vehicle-treated nude mice. The lower expression (URB602-treated mice) 27.13 Cq vs background N/A Cq was put= 1.

**Figure 5.** Representative images of CD31 immunostaining (upper) or immunofluorescence (bottom) in tumor sections from untreated (Ctrl) and URB602-treated mice (URB602). Scale bars indicate 100 (upper) or 50 (bottom) μm. Images obtained by fluorescence microscope (Eclipse TE300, Nikon) at 20x (upper) or 40x (bottom) magnification and taken by a digital Q10 camera. Bar graph represents the number of CD31 positive vessels, calculated counting 8 random fields/section for slides, each slide having five sections. URB602 (5 mg/kg, i.p.) treatment started 10 days after cell inoculation and it was administered every day until the sacrifice of the animals. Assays were performed 8 days after the first injection of URB602. Results are mean ± SEM tumors from three different mice. Each experiment was in triplicate. ***P<0.001 *vs* vehicle-treated nude mice.

**Figure 6.** Effect of URB602 on cell proliferation (figure 6A) and on cell migration (figure 6B) in HUVEC under basal condition (0.1% FCS) or in cells stimulated for 24 h with either 1% FCS or FGF-2 (20 ng/ml).

(A) URB602 (0.1–1 μM) was added to the cell media 30 min before stimulation. Data are expressed as counted cells/well ± SEM from 4 independent experiments. **p<0.01 and ***p<0.001 *vs* 0.1%

FCS URB602-untreated cells, $^{\S}p<0.05$ and $^{\S\S\S}p<0.001$ *vs* 1% FCS URB602-untreated cells; $^{\#\#}p<0.01$ *vs* FGF-2 URB602-untreated cells. (B) Top. Effect of URB602 (1μM) in HUVEC monolayers. URB602 was added to the cell media 30 min before stimulation. The graph shows % change in wound area.*p<0.05 and ***p<0.001 vs. 0.1% FCS URB602-untreated cells, $^{\#}p<0.05$ vs. 1% FCS URB602-untreated cells and $^{\S\S\S}p<0.001$ vs. FGF-2 URB602-untreated cells. (B) Bottom. Representative pictures (of 4 experiments) of Hoechst 33342 labelled cells.

**Figure 7.** Effect of the MAGL lipase inhibitor URB602 (1μM) on FGF-2 (A) and endostatin levels (B) in HUVEC under basal condition (0.1% FCS) or in cells stimulated for 18 h with either 1% FCS or FGF-2 (20 ng/ml). Data are reported as pg/ml (FGF-2) or ng/ml (endostatin) (means ± SEM) from 3 independent experiments (in triplicate). ***p<0.001 vs. 0.1% FCS URB602-untreated cells, ##p<0.01 and $^{\#\#\#}p<0.001$ vs 1% FCS URB602-untreated cells.

**Figure 8.** Chemopreventive effect of URB602 in the azoxymethane (AOM) model of colon carcinogenesis. Figures 7A-C report the inhibitory effect of URB602 on aberrant crypt foci (ACF) (A), polyps (B) and tumors (C) induced in the mouse colon by AOM. URB602 (5 mg/kg, i.p.) was given three times a week for the whole duration of the experiment starting 1 week before the first administration of AOM. Measurements were performed 3 months after the first injection of AOM. The criterion to distinguish polyps from tumors was established considering the main characteristic features of these two lesions (i.e. crypt distortion around a central focus and increased distance from luminal to basal surface of cells for polyps and high grade of dysplasia with complete loss of crypt morphology for tumors) [37]. Results represent the mean ± SEM. of 9-11 mice.*P<0.05 and **P<0.01 vs AOM alone.

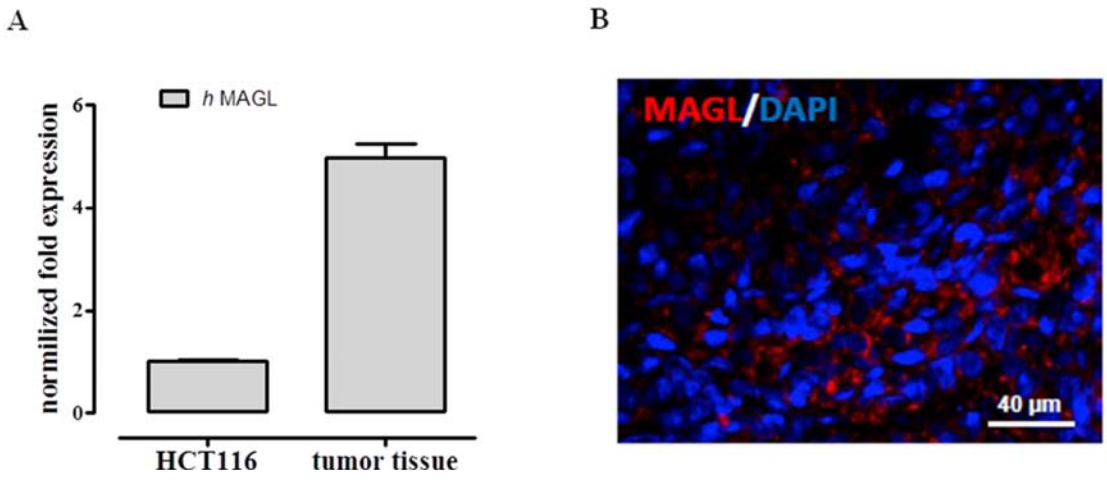


**Figure 1**

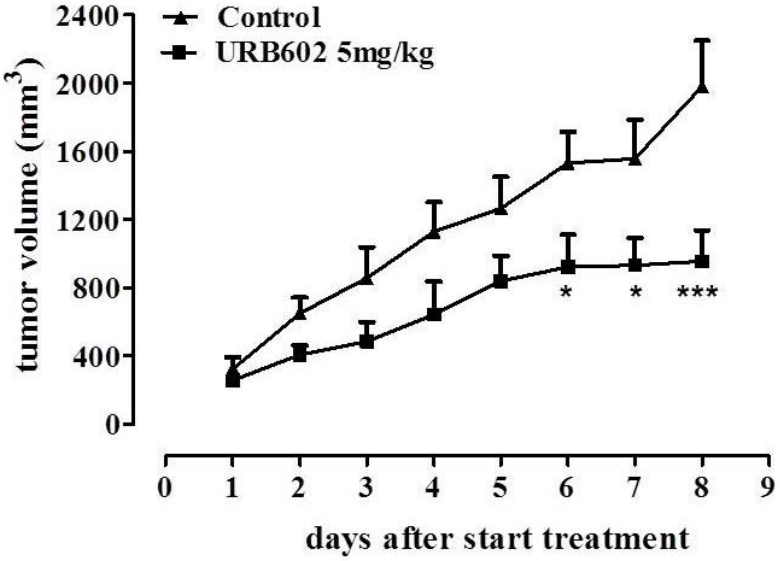


**Figure 2**

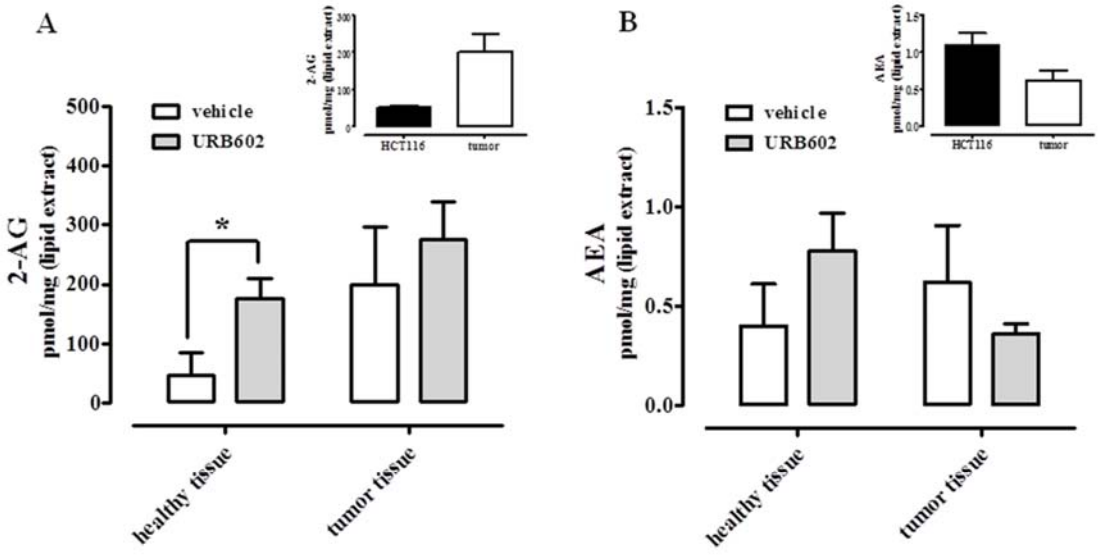


Figure 3

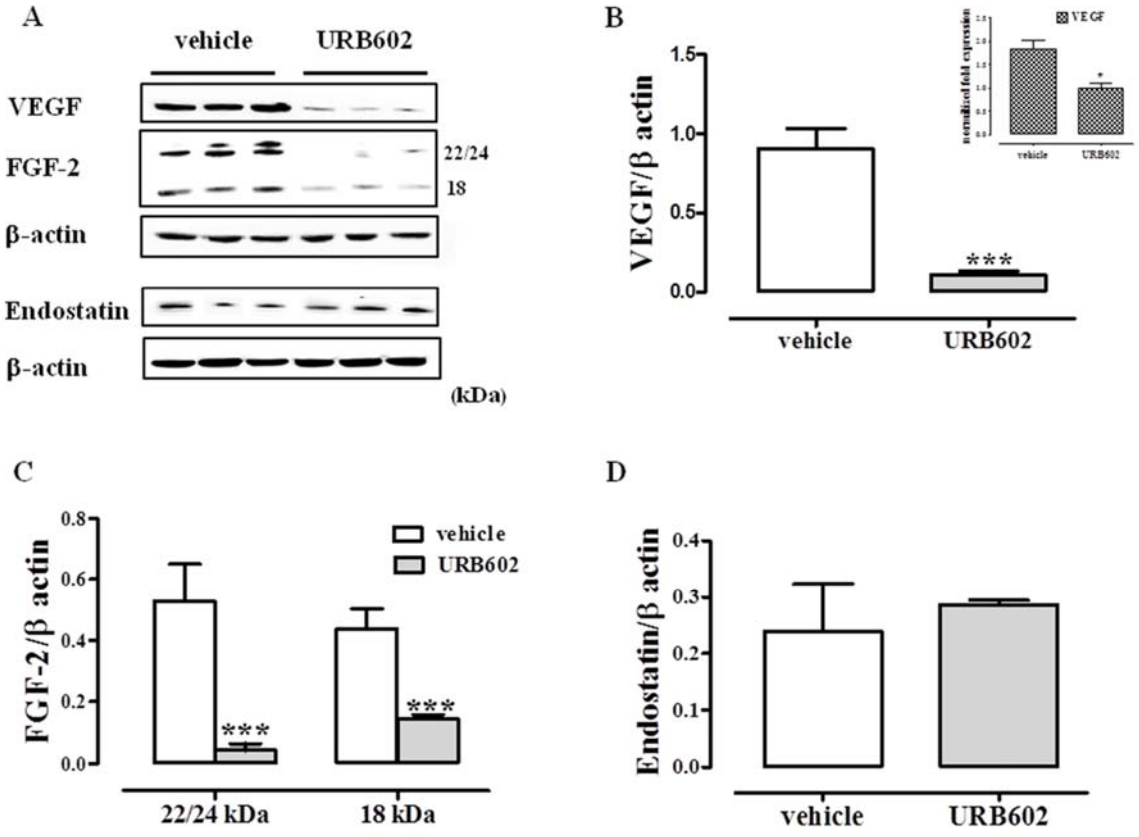


Figure 4

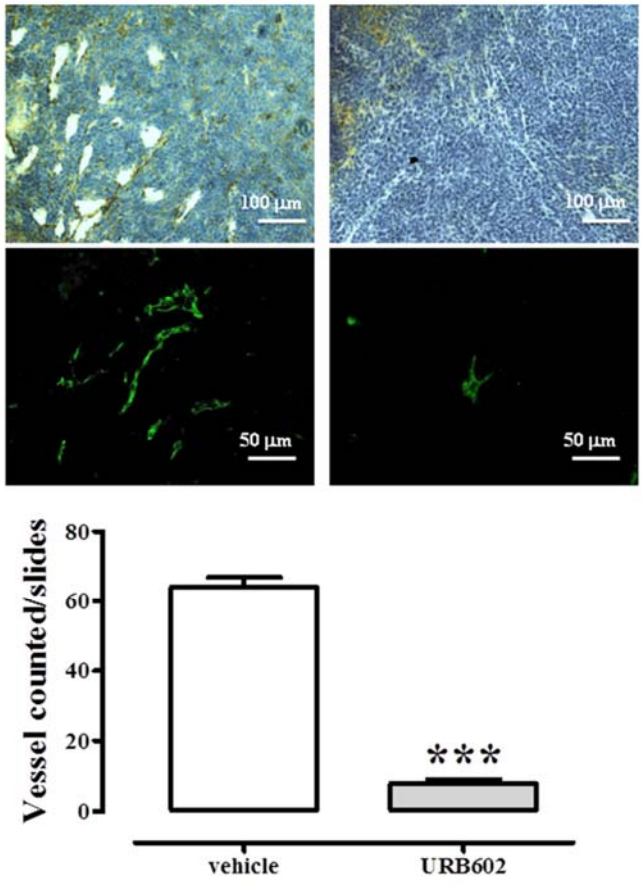


Figure 5

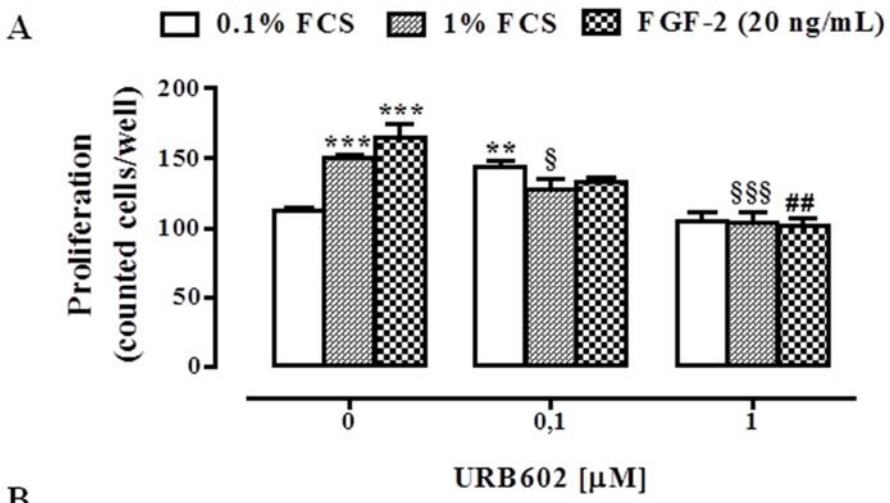


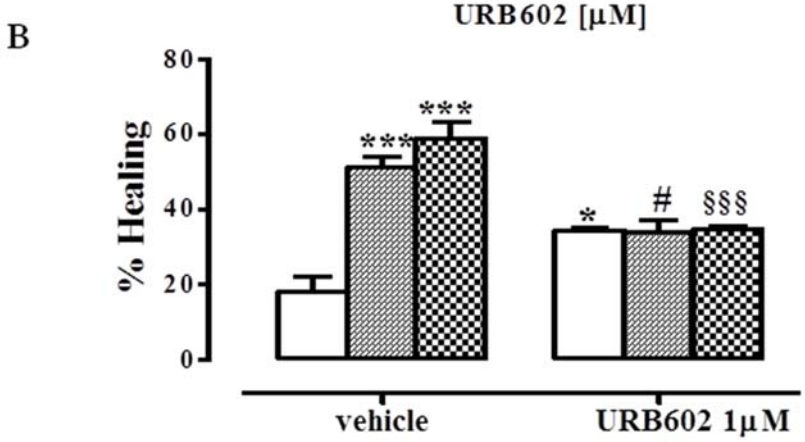


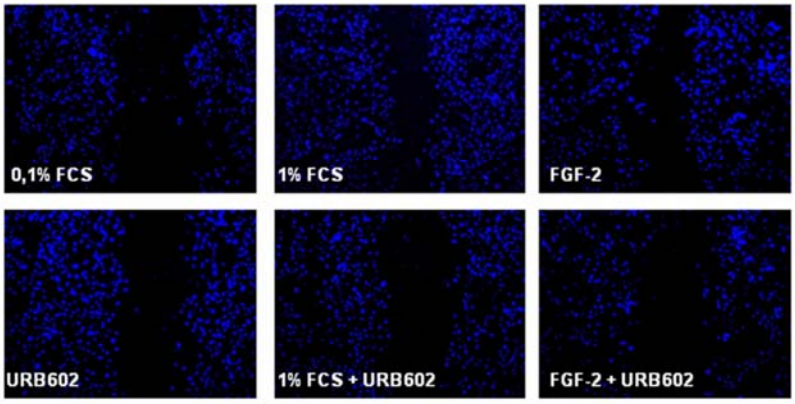


Figure 6

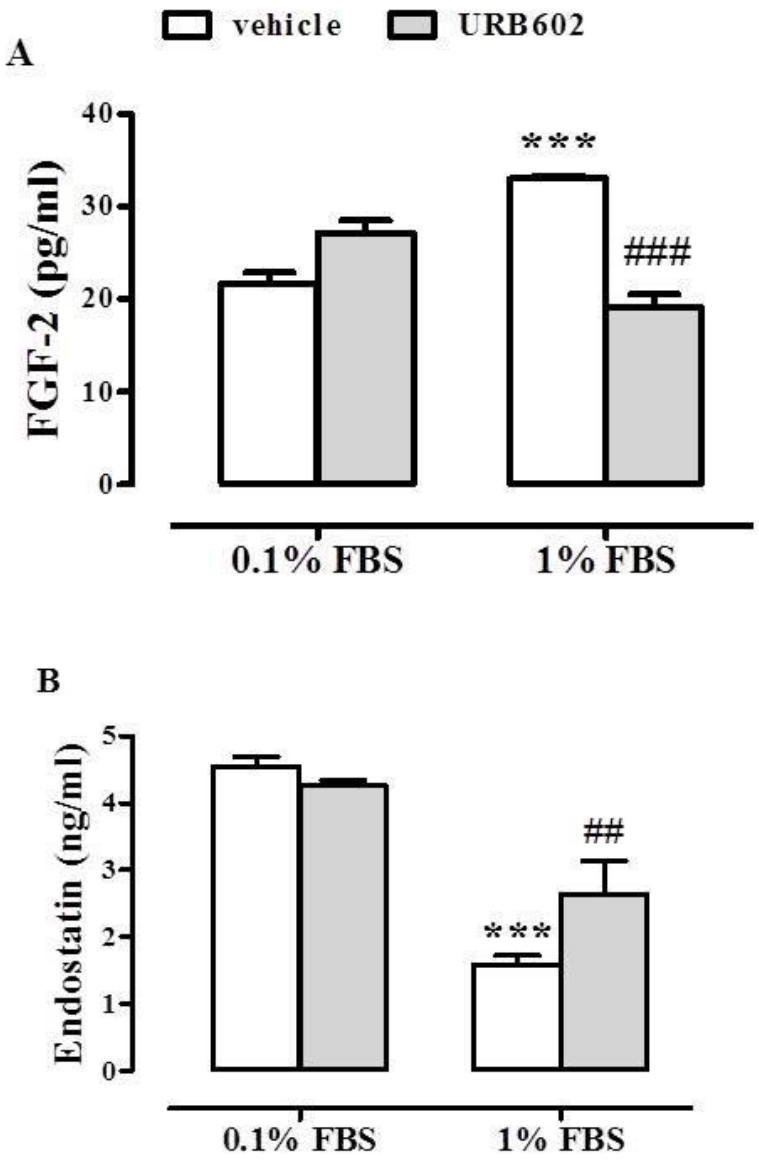


**Figure 7**

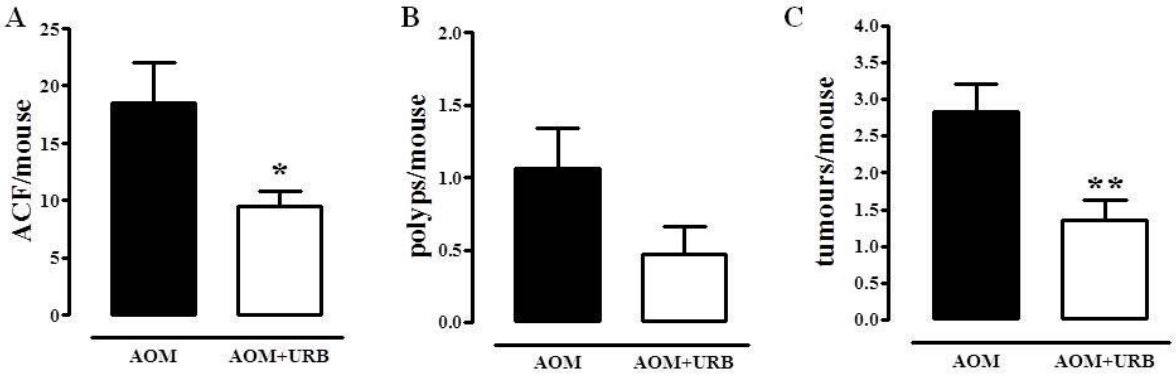


**Figure 8**